NEUROSCIENCE

Neuronal control of maternal provisioning in response to social cues

Jadiel A. Wasson[1†], Gareth Harris[2,3†], Sabine Keppler-Ross[1], Trisha J. Brock[4], Abdul R. Dar[5], Rebecca A. Butcher[5], Sylvia E. J. Fischer[6], Konstantinos Kagias[2], Jon Clardy[7], Yun Zhang[2]*, Susan E. Mango[1]*

Mothers contribute cytoplasmic components to their progeny in a process called maternal provisioning. Provisioning is influenced by the parental environment, but the molecular pathways that transmit environmental cues between generations are not well understood. Here, we show that, in *Caenorhabditis elegans*, social cues modulate maternal provisioning to regulate gene silencing in offspring. Intergenerational signal transmission depends on a pheromone-sensing neuron and neuronal FMRFamide (Phe-Met-Arg-Phe)–like peptides. Parental FMRFamide-like peptide signaling dampens oxidative stress resistance and promotes the deposition of mRNAs for translational components in progeny, which, in turn, reduces gene silencing. This study identifies a previously unknown pathway for intergenerational communication that links neuronal responses to maternal provisioning. We suggest that loss of social cues in the parental environment represents an adverse environment that stimulates stress responses across generations.

INTRODUCTION

A key question in biology is how animals help their progeny survive in the face of environmental challenges. One tactic is to optimize maternal provisioning to prepare offspring for the environmental conditions they will encounter. For example, when food is scarce, *Caenorhabditis elegans* mothers increase deposition of vitellogenins in oocytes, and these vitellogenins provide an internal energy source that supports larval development (*1*). Although regulators of vitellogenin synthesis have been discovered, the conduit from environment to maternal deposition is unknown. Here, we identify a role for neuronal signaling that interprets and transmits environmental cues for maternal provisioning. Previous studies implicated neurons for producing small RNAs that can be inherited, using transgenic manipulation (*2*, *3*), but a natural role for neurons has not been shown. We uncover a role for a chemosensory neuron and a neuronal FMRFamide (Phe-Met-Arg-Phe)–related signal for modulating maternal provisioning of translational machinery to withstand adverse conditions.

RESULTS

We sought to identify factors involved in communication from the parental environment to progeny in *C. elegans*. Environmentally supplied double-stranded RNA (dsRNA) induces gene silencing in the next generation, providing a useful assay (*4*). We fed mothers diluted dsRNA for the essential gene *pha-4*, which generated weak silencing in the progeny in wild-type animals, and screened for mutants that enhanced RNA interference (RNAi) potency. Silencing

was monitored as lethality of the progeny after *pha-4(RNAi)* (Fig. 1A) or reduced PHA-4 expression (see below). We found that the strength of RNAi was enhanced in mutants that were defective in pheromone biosynthesis: Mutations in *daf-22/SCP2*, *dhs-28/HSD*, or *acox-1.1/ACOX1* (*5–8*) each generated more lethality compared to wild-type worms (Fig. 1B). Of these, *dhs-28* was somewhat variable. Previous studies have shown that long-term cultures of *dhs-28* mutant animals accumulated dauer-inducing activity in the culture medium due to the production of long-chain ascarosides stalled at a particular step in the β-oxidation process (*6*). These and related compounds may modify the *pha-4(RNAi)* phenotype and contribute to the variability in the effects generated by inactivating *dhs-28*. In summary, these mutants implicate pheromones in tamping down RNAi.

Addition of conditioned medium made from wild-type animals restored the RNAi response of *daf-22* mutants, but the addition of conditioned medium from *daf-22* mutants did not (Fig. 1B). This result indicates that RNAi in progeny responds to molecules synthesized by the *daf-22* pathway and secreted into the environment. Moreover, exposure to conditioned medium for 24 hours during the last larval stage and early adulthood was sufficient for rescue, indicating that early life exposure of parents to environmental cues was not necessary. The *daf-22* pathway generates multiple pheromones that signal the presence of conspecifics, including ascarosides asc-ωC3, asc-C6-MK, and asc-ΔC9, which induce a developmental arrest (dauer) when present in high concentrations (*7*, *9*, *10*). However, a synthetic mixture of these three dauer pheromones, which are highly effective in inducing dauers under established conditions (*7*, *9*, *10*), did not rescue the enhanced RNAi of *daf-22* mutants (fig. S1E). These data suggest that RNAi in progeny is modulated by exposure of mothers to conspecific pheromones in the environment, and these are distinct from dauer pheromones.

Small-molecule pheromones are detected by chemosensory neurons, including ADL, ASK, and ASI (*11–16*). We discovered that killing the ASI neurons enhanced RNAi in the progeny, whereas killing or blocking neurotransmission of ADL, ASK, or several other sensory neurons did not (Fig. 1C; we note that ASK may promote

[1]Biozentrum, University of Basel, Basel, Switzerland. [2]Department of Organismic and Evolutionary Biology, Center for Brain Science, Harvard University, Cambridge, MA, USA. [3]Department of Biology, California State University Channel Islands, Camarillo, CA, USA. [4]InVivo Biosystems, Eugene, OR, USA. [5]Department of Chemistry, University of Florida, Gainesville, FL, USA. [6]Division of Infectious Diseases, Boston Children's Hospital, Boston, MA, USA. [7]Department of Biological Chemistry and Molecular Pharmacology, Harvard Medical School, Cambridge, MA, USA.
*Corresponding author. Email: susan.mango@unibas.ch (S.E.M.); yzhang@oeb.harvard.edu (Y.Z.)
†These authors contributed equally to this work.
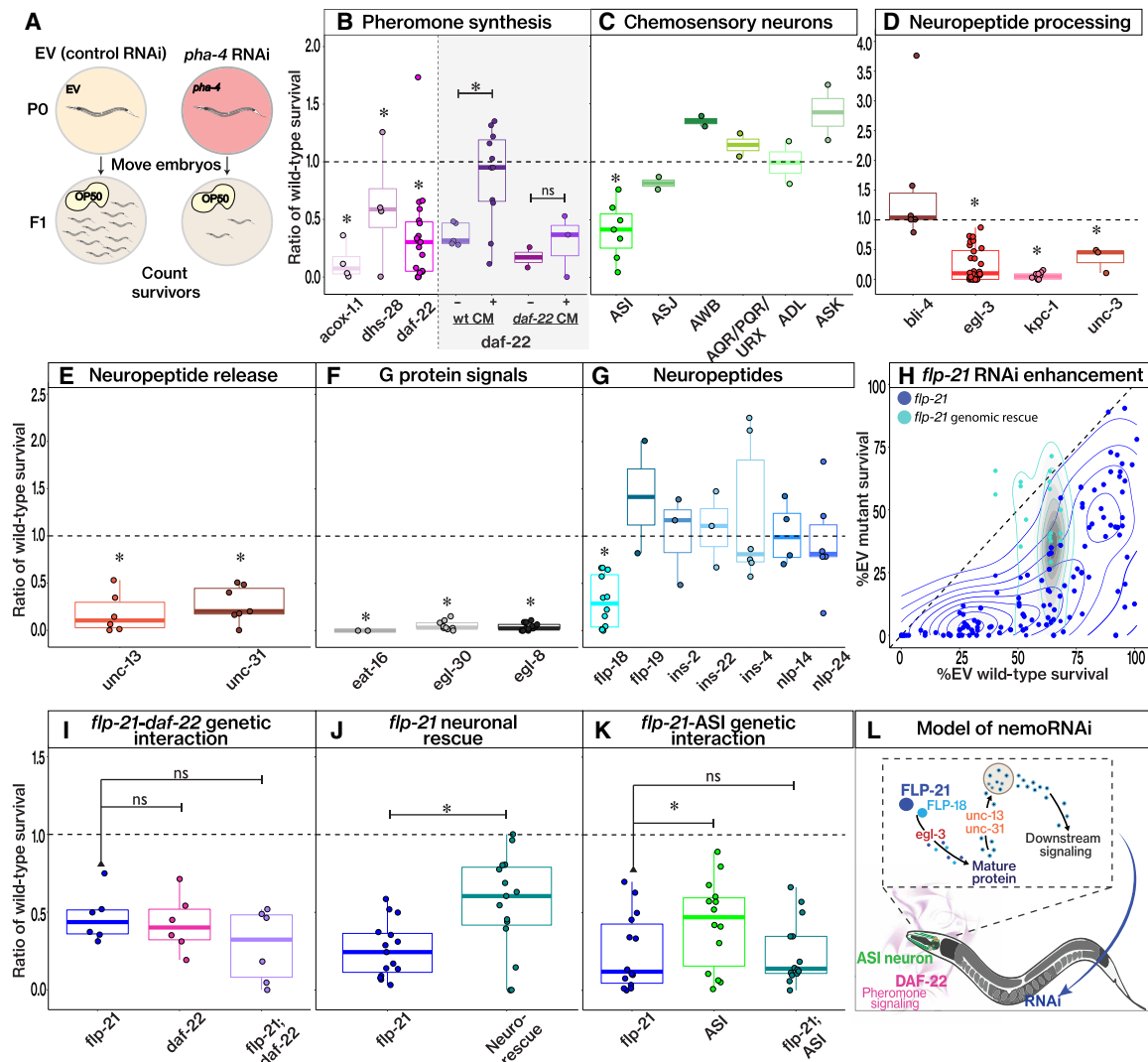
Fig. 1. Neuronal signaling modulates RNAi. (**A**) Schematic of *pha-4* RNAi survival experiments. Survey for enhanced RNAi by genes involved in (**B**) pheromone synthesis, (**C**) chemosensory neurons, (**D**) neuropeptide processing, (**E**) neuropeptide release, (**F**) G protein signals, (**G**) neuropeptides, and (**H**) *flp-21*. Enhanced RNAi is rescued by (B) conditioned medium (CM) from wild-type animals (wt CM) but not from *daf-22* mutants (*daf-22* CM), (H) a genomic transgene for *flp-21* for *flp-21(ok889)*, or (J) a neuronally expressed *flp-21* for *flp-21(ok889)*. Epistasis analysis between *flp-21* and (**I**) *daf-22* or (**K**) loss of ASI generated by caspase expression. (**L**) Model for nemoRNAi. Environmental signals such as pheromones (pink) signal through chemosensory neurons such as ASI (green). FLP-21 and FLP-18 neuropeptides (dark and light blue) are processed (red) and released (orange). Target cells activate G protein signaling cascades (black). These pathways converge on RNAi regulation in the developing embryo. Data visualization represents the ratio of wild-type %EV survival for each mutant (wild type represented by a dotted line at 1 on each graph). Boxplots indicate the first quartile (Q1) to Q3, with box, median, and Q2 of data indicated by a horizontal line, and whiskers go from Q1 to smallest non-outlier and from Q3 to largest non-outlier. Each boxplot represents at least two biological replicates. Individual experiments represented as points on boxplots. *$P < 0.05$. ns, not significant. The details of the data analysis are included in Materials and Methods.

RNAi, as its loss leads to better survival). To confirm the role of ASI, we inactivated *unc-3*, which encodes a transcription factor required for ASI cell fate (*17*, *18*), and observed enhancement of *pha-4(RNAi)* (Fig. 1D). Next, we examined components involved in ASI-related signaling, including *egl-3* and *kpc-1*, which encode pro-protein convertases that process signaling peptides (*19*, *20*). Mutations in either of these genes enhanced RNAi, whereas the endoprotease *bli-4* did not (Fig. 1D) (*21*, *22*). *unc-13*, which is required for peptide and vesicle release during neurotransmission (*21*, *23*), enhanced RNAi when mutated. *unc-31*, which encodes a calcium-dependent activator

protein that regulates the release of signaling peptides from dense core vesicles (*24*), also enhanced RNAi when mutated (Fig. 1E).

The requirement for the ASI neuron, as well as *egl-3*, *kpc-1*, *unc-13*, and *unc-31*, implicated neuropeptides in maternal modulation of RNAi. Neuropeptides fall into three categories, the FMRFamide-like peptides (FLPs), the insulin-like peptides (ILPs), and the neuropeptide-like peptides (NLPs) (*21*). We surveyed candidates from all three categories and discovered that two FLP genes, *flp-18* and *flp-21* (*25*, *26*), were involved in modulating RNAi in progeny. Two mutant alleles of *flp-18* and *flp-21* enhanced RNAi (Fig. 1, G and H)

and did so over a range of dsRNA dilutions (Figs. 1H and 2A). These results suggest nonredundant functions for these two neuropeptides in regulating the *pha-4(RNAi)* effects on offspring. In contrast, inactivation of several ILPs or NLPs showed no effect, although insulin signaling has been implicated in other examples of intergenerational communication (*27–29*).

Expressing a genomic fragment containing the wild-type *flp-21* gene rescued the enhanced RNAi phenotype (Fig. 1H). RNAi enhancement was also rescued by a single-copy transgene expressing *flp-21* broadly in neurons (Fig. 1J) (*30*). We observed an intermediate level of rescue, which may reflect variable expression of the promoter in neurons, effects of neuronal specificity, or an additional nonneuronal function of *flp-21* as part of the mechanism. Nonetheless, these data support a neuronal focus in which *flp-21*–mediated signaling in neurons modulates the strength of RNAi in the next generation; we focus on *flp-21* for the remainder of the study.
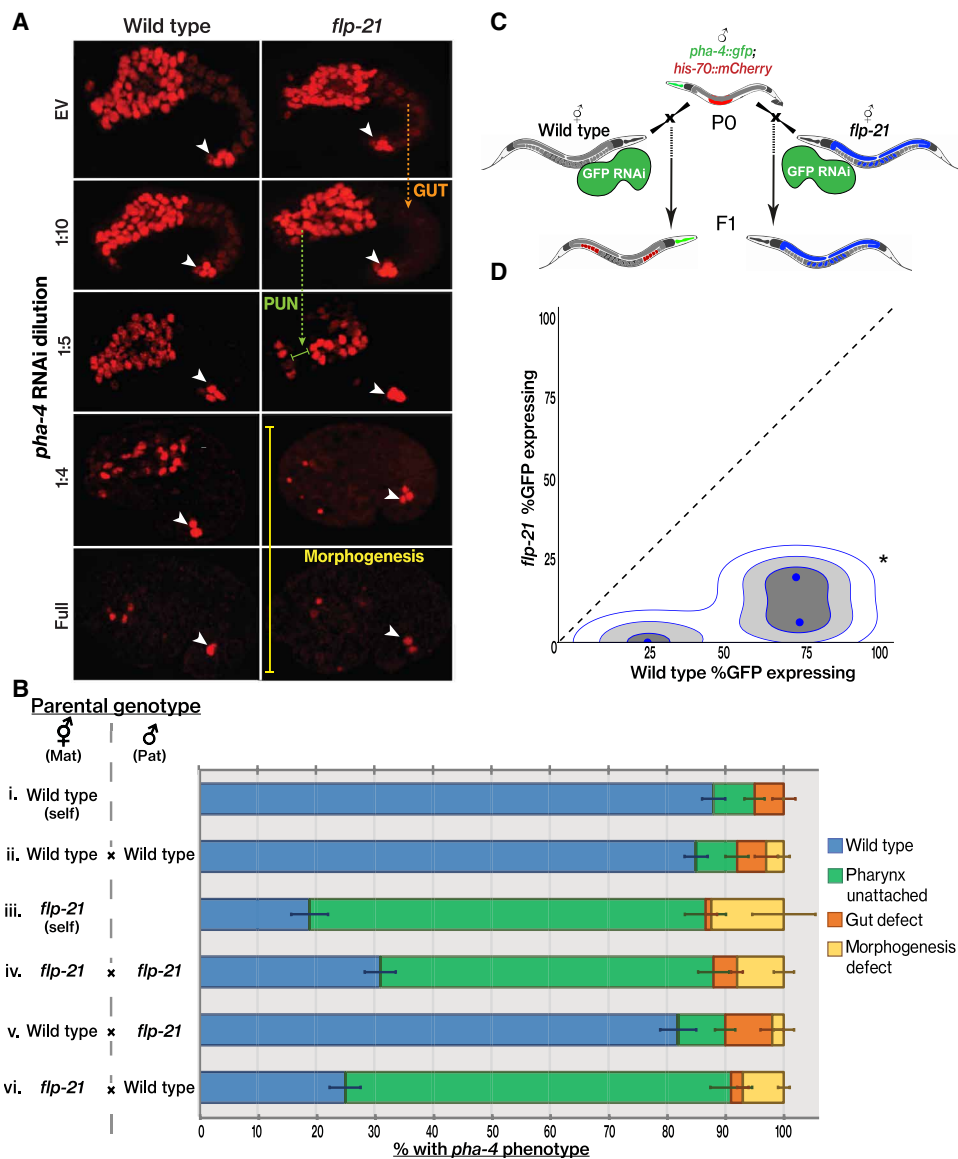
Fig. 2. NemoRNAi is maternal and does not require the target locus. (**A**) PHA-4 protein in wild-type or *flp-21* embryos treated with varying dilutions of dsRNA. Phenotypes of gut defects (GUT), pharynx unattached (PUN), and morphogenesis denoted by orange, green, and yellow, respectively. Note the hindgut stains in all samples, a positive staining control because it is refractory to RNAi (arrow). (**B**) Self-progeny (i and iii) or progeny from mating (ii and iv to vi) were examined for *pha-4* phenotypes after RNAi. Mother (Mat) and father (Pat). Quantitation of *pha-4* phenotypes (wild type in blue, PUN in green, gut defective in orange, and morphogenesis defect in yellow) in progeny from each of the indicated crosses reveals that *flp-21* mutation is required in mothers. Most marked phenotype is graphed. Error bars indicate SD across three biological replicates. (**C**) Schematic of cross to determine whether target DNA is required in mothers for enhancement. Wild type or *flp-21* mutants lacking a *gfp* transgene are exposed to *gfp* dsRNA and then mated to *pha-4::gfp* males (with linked *his-70::mcherry* to identify cross progeny). (**D**) Graph of data from (C) indicating percent progeny expressing green fluorescent protein (GFP) from wild-type (*x* axis) or *flp-21* (*y* axis) mothers (each point is the average GFP expression from the total number of progeny in one paired experiment; three biological replicates were performed). Dotted line represents 1:1 GFP expression in wild-type versus *flp-21* progeny. Wilcoxon rank sum, *P < 0.05.

To investigate the extent and gene specificity of *flp-21* beyond *pha-4(RNAi)*, we surveyed dsRNAs targeting a variety of genes. *flp-21* mutants exhibited an enhanced RNAi response to a range of dsRNAs, including those targeting maternally expressed genes (*mex-3* and *skn-1*) and genes activated during the first half of embryonic development (*dlg-1*, *par-3*, *hmr-1*, and *pha-4*) (Fig. 2A and fig. S1A). However, two genes expressed during terminal embryogenesis were resistant to RNAi in the wild type and failed to be enhanced by *flp-21* (*ifb-2* and *myo-2*) (fig. S1A). Likewise, terminal *pha-4* expressed in the hindgut was refractory to RNAi, presumably because it is activated late (e.g., Fig. 2A). We also found that *flp-21* mutants enhanced RNAi over a range of dsRNA exposure, from 18 to 43 hours (fig. S1B). These data indicate that loss of *flp-21* results in a generally enhanced RNAi ("Eri") phenotype for genes expressed during early embryo development. We call this Eri phenotype neuronal enhancement by mother of RNAi ("nemoRNAi"; Fig. 1L).

FLPs signal to target tissues via G protein–coupled receptor signaling cascades (*31*). We found that EGL-30, the Gq-protein subunit α (*32*), induced a nemoRNAi phenotype when inactivated (Fig. 1F). Furthermore, mutations in *eat-16*, a regulator of G protein signaling, and *egl-8*/PLCβ, an additional signaling component of Gαq pathways (*32*, *33*), both had nemoRNAi phenotypes when exposed to diluted *pha-4* dsRNA (Fig. 1F). Together, these results suggest that Gαq signaling plays a role in nemoRNAi mediated by FMRFamide-like neuropeptide FLP-21.

Epistasis analysis between *flp-21* and *daf-22* indicated that these two factors act in the same pathway because double mutants did not produce an additive effect (Fig. 1I). Similarly, *flp-21* mutations combined with ASI removal indicated that these also act in the same pathway (Fig. 1K). These data suggest that a pheromone-responsive, FLP-specific chemosensory signaling pathway modulates gene silencing in progeny via RNAi (Fig. 1L). We conclude that sensory perception, including that of social information, modulates silencing in progeny. We focus on *flp-21* for the remainder of the study, given its robust phenotype and lack of pleiotropy.

If FLP-21 links pheromone sensing to gene silencing in progeny, it predicts that FLP-21 functions in parents, not progeny. To test this idea, we examined the phenotypes of heterozygous F1 progeny generated by mating mutant and wild-type parents. Mutant *flp-21* mothers mated with wild-type fathers produced progeny that behaved like *flp-21* homozygotes (Fig. 2B, compare row vi with rows iii and iv), whereas wild-type mothers mated with mutant fathers produced offspring that behaved like wild-type (Fig. 2B, compare row v with rows i and ii). These data reveal that *flp-21* functions in mothers to modulate the RNAi response in progeny. We note that *flp-21* is expressed in the soma and is not contributed to the embryo from the mothers' germ lines (*34*). These data support the hypothesis that the FLP-21–mediated signaling pathway acts in mothers to modulate RNAi in progeny (see Discussion).

Given that chromatin modifications have been implicated in communication between mothers and offspring (*35*), we tested whether the target gene of nemoRNAi had to be present in mothers, a condition required for chromatin modification in *cis*. Wild-type or *flp-21* mutant mothers were exposed to dsRNA against *gfp* and mated to males bearing a *gfp* transgene (Fig. 2C). The resulting progeny carried the paternal *gfp* transgene with a linked *histone::mCherry* control (Fig. 2C). *flp-21* mutations enhanced *gfp* silencing in progeny, revealing that the target *gfp* gene was not required in

mothers to initiate nemoRNAi (Fig. 2D). We conclude that chromatin modifications at the target locus are not required for *flp-21*–dependent intergenerational communication. We recognize that indirect effects of chromatin modifications may still be involved.

Because nemoRNAi did not require the target locus in mothers, a diffusible molecule such as RNA was an attractive candidate to be the vehicle of inheritance. We focused on mRNAs that differed between wild-type and *flp-21*, as maternal deposition of mRNA regulates many aspects of embryogenesis (*36*, *37*). We isolated RNA from early embryos, at a stage when RNA is maternally provided (*38*), and performed differential expression analysis to identify 3791 significantly deregulated genes in *flp-21* early embryos compared to wild type (Fig. 3A and table S3). These genes were enriched for translation/ribosomal components according to four categories of Gene Ontology (GO) term analysis: Biological Pathway, Cell Component, Molecular Function, and KEGG (Kyoto Encyclopedia of Genes and Genomes) Pathway (Fig. 3B). Moreover, two ribosomal RNAs, *rrn-3.1* and *rrn-1.2*, and the elongation factor *eef-1A.1* were the top drivers distinguishing wild-type from *flp-21* RNA samples by two-dimensional (2D) principal components analysis (PCA; Fig. 3C). Additional differences between our RNA samples included vitellogenins (PCA), innate immunity (GO analysis), and protein phosphorylation (GO analysis), but only translational components were identified as top hits by both GO analysis and PCA.

We generated circle plots for the top eight GO pathways to identify the directionality of the RNA changes within each GO category (fig. S2A). In each category, there was a robust down-regulation of translation-associated terms. These results were confirmed by quantitative polymerase chain reaction (qPCR) analysis for eight translation machinery genes spanning initiation, elongation, termination, and the ribosome itself (Fig. 3D); a ninth gene, *ifet-1*, was up-regulated in *flp-21* mutants and encoded a translation inhibitor (Fig. 3D) (*39*). In addition, single-molecule fluorescence in situ hybridization (smFISH) for ribosomal protein *rpl-7* revealed an almost twofold decrease in *flp-21* mutants (Fig. 3, E and F). Together, these data indicate that many maternally provided translation components are reduced in *flp-21* early embryos.

The reduction of translation components in *flp-21* early embryos suggested a decrease in translation rate. To test this idea, we analyzed translation in wild-type and *flp-21* mutants with ^{35}S metabolic labeling. ^{35}S incorporation was reduced to less than 50% in *flp-21* mutants compared to wild-type animals, which was comparable to well-known translation-deficient mutants *rsks-1* and *eat-2* (Fig. 4A) (*40*). This result revealed that the ongoing translation rate in *flp-21* mutants was reduced significantly. We note that, despite the reduced translation, PHA-4 protein expression was normal in *flp-21* mutants in the absence of *pha-4(RNAi)*, and these mutants had wild-type pharyngeal pumping, as did other nemoRNAi mutants (Fig. 2 and fig. S1, C and D). Thus, *flp-21* mutants are healthy, despite lower rates of translation.

We next asked whether the translational changes of *flp-21* mutants could account for nemoRNAi. Because many genes associated with translation are embryonic lethal, we relied on heterozygous mutations for some genes and surveyed these by *pha-4(RNAi)*. From our panel of mutants, four had enhanced lethality: *inf-1*, *ifet-1/+*, *iff-2/+*, and *rpl-7/+* (Fig. 4B). Of these, *iff-2/+* and *rpl-7/+* mothers generated a reduction of PHA-4 staining that closely resembled that of *flp-21* mutants (Fig. 4C and fig. S2C). *inf-1* and *ifet-1* were both sickly, even for the empty vector (EV) control, so a possible role was
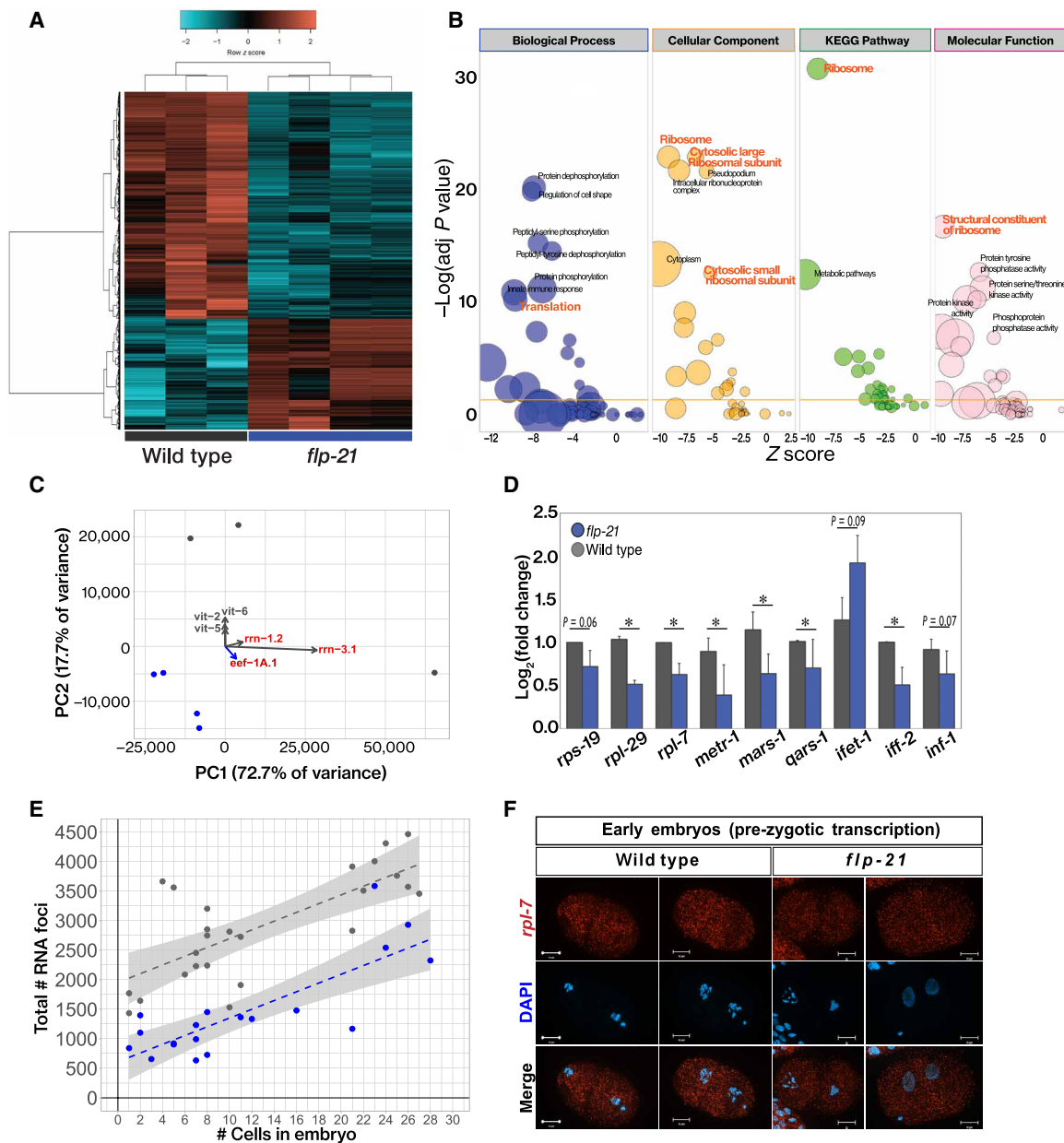
Fig. 3. RNA sequencing reveals down-regulation of translation components in *flp-21* mutants. (**A**) Heat map and hierarchical clustering of significant transcriptional changes revealed by DESeq2 for three wild-type and four *flp-21* replicates (red, up-regulated genes; turquoise, down-regulated genes; z scores were indicated). (**B**) Bubble plots for GO analysis enriched terms identified with DAVID [significant genes from (A)]. Four different categories of GO analysis and KEGG pathways were indicated. Size of bubbles indicates the number of genes. The x axis indicates z score, and the y axis indicates negative logarithm of adjusted *P* value from GO analysis (higher = more significant). GO analysis enriched terms with log(adjusted *P* value) < 10 labeled with ID. Translation and ribosomal components are top hits in each GO category and in KEGG pathways. (**C**) PCA analysis of wild-type (gray circles) and *flp-21* (blue circles) samples. The top genes driving clustering of samples are labeled, and arrows indicate direction of driving change. PC1 on x axis, and PC2 on y axis. (**D**) qPCR confirmation of select translational machinery components. Two samples from each genotype were assayed in three independent experiments. Data presented as log$_2$(fold change). Statistics performed on ΔΔC$_t$ values, ANOVA Tukey's, *P < 0.05. (**E**) Quantitation of sm-FISH for wild-type and *flp-21* mutants. The x axis represents embryonic age (no. of cells), and the y axis represents the number of smFISH foci. (**F**) Representative smFISH (red) images for *rpl-7* (scale bars, 10 μm).

less clear for these genes (fig. S2D). These data suggest that not all translational components could modulate RNAi efficiency, but that reduction of *iff-2* and *rpl-7* was particularly effective for enhancing RNAi. *rpl-7* is a conserved portion of the 60S ribosome (*41*). *iff-2* encodes the ortholog of mammalian EIF5A and EIF5A2 (*42*). EIF5A is important both for translational elongation, particularly at ribosome

stalling sites, and for termination (*43*). EIF5A2 may also function in mRNA decay in response to stress (*44*), and both factors have been implicated in human diseases such as cancer (*45*).

If the reduction in translation is sufficient to explain nemoRNAi in *flp-21* mutants, then a combination of mutations should not have an additive effect on lethality associated with *pha-4(RNAi)*. This
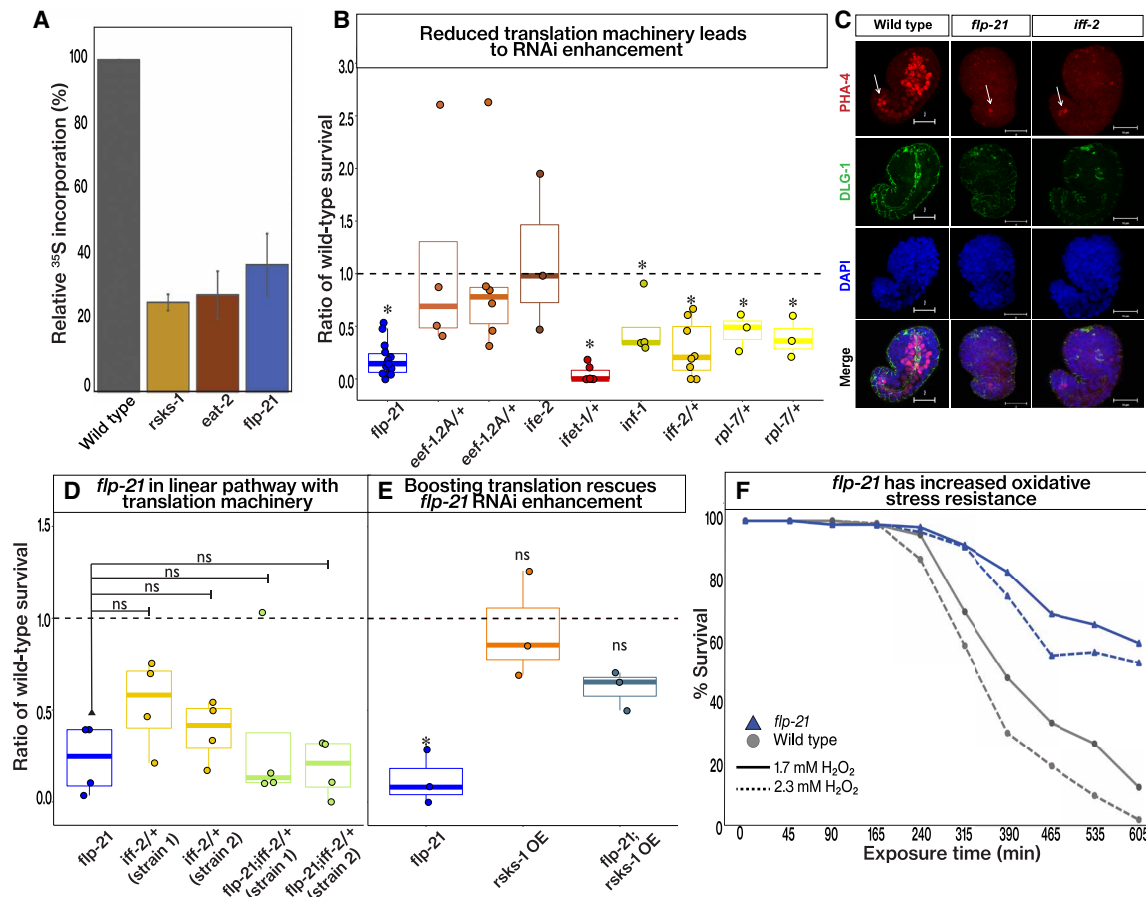
Fig. 4. Translation is reduced in *flp-21* mutants and sufficient for nemoRNAi. (**A**) Relative ^{35}S incorporation. Wild type set to 100%. *flp-21* mutants have reduced incorporation rates compared to wild type. Positive controls for reduced translation are *rsks-1* and *eat-2*. ANOVA Tukey's, *$P < 0.05$. (**B**) *pha-4(RNAi)* survival assay performed on translation machinery genes. Data visualization represents ratio of wild-type %EV survival for each mutant (wild type represented with dotted line at 1 on each graph). Four mutants (*inf-1*, *ifet-1/+*, *iff-2/+*, and *rpl-7/+*) in addition to *flp-21* have an enhanced RNAi phenotype. Note hindgut staining (arrow). (**C**) Representative images of PHA-4 staining after *pha-4(RNAi)* for indicated genotype (scale bars, 10 μm). Note the hindgut stains in all samples, a positive staining control because it is refractory to RNAi. (**D**) Genetic interaction between *flp-21* and *iff-2* heterozygotes reveals that they are in the same pathway. (**E**) Genetic interaction between *flp-21* and *rsks-1* overexpression (OE) transgene rescues enhanced RNAi phenotype. ANOVA Dunnett's test, *$P < 0.05$. (**F**) Oxidative stress assay. % Survival is assayed over 565 min for wild type and *flp-21*. Solid line indicates assay performed with 1.7 mM H_2O_2. Dotted line indicates assays performed at 2.3 mM H_2O_2. *flp-21* mutants in blue, and wild type in gray.

prediction was borne out: *flp-21; iff-2/+* double mutants resembled *flp-21* single mutants for the response to RNAi (Fig. 4D). We analyzed two independently constructed strains of *flp-21; iff-2/+* along with single mutant strains for *iff-2/+* (two strains) and *flp-21* (one strain) generated from the siblings during the strain construction. The combination of *flp-21* mutations with a heterozygous *iff-2* allele resulted in no additive effect on RNAi lethality, indicating that these two genes are in the same pathway for nemoRNAi.

Pathways that regulate translation converge on Target of Rapamycin (TOR) components and S6 kinase signaling, which includes LET-363 and RSKS-1 in *C. elegans* (*46*). To determine whether translation was key for nemoRNAi by *flp-21* mutations, we introduced an *rsks-1* overexpression transgene into the *flp-21* mutant background. Augmenting translation via *rsks-1* overexpression (*47*, *48*) was able to rescue the enhanced RNAi phenotype of *flp-21* progeny (Fig. 4E). Because we have demonstrated that these maternal chemosensory pathways interact with, and respond to, environmental cues, this work suggests a model where the maternal environment

can modulate embryonic gene silencing and development via provisioning of translation components.

Our next goal was to determine the physiological consequences of *flp-21* loss in the absence of RNAi. Because both regulation of translation and RNAi mechanisms have been linked to stress responses in worms (*49–52*), we exposed worms to different degrees of oxidative stress (hydrogen peroxide; Fig. 4F). Within 5 hours, wild-type animals exhibited classic oxidative stress responses including muscle rigidity. By 10 hours, wild-type worms were largely dead. By contrast, more than 50% of *flp-21* mutant animals were still alive by the end of the time course and were still actively mobile, indicating resistance to oxidative stress. These data suggest that *flp-21* mutants are primed to withstand stress.

DISCUSSION
The link between pheromones and stress pathways suggests that worms use pheromones from conspecifics to gauge the quality of

the environment. A high concentration of certain pheromone compounds is known to represent poor conditions (crowding and lack of food) (*6*, *9*, *53*). Here, we show that worms respond to other pheromones in a positive way. Their absence is an indication that the environment harbors something detrimental for *C. elegans*—too little food or the presence of a toxin or pathogen perhaps. Worms begin to prepare offspring for this unseen challenge by reducing energy-intensive processes like translation and heightening stress responses. FLP-21 is known to regulate acute behavioral response to environmental stress, such as adverse oxygen concentrations (*26*, *54*). In vertebrates, neuropeptides coordinate the nervous system and the immune system to generate integrated responses to stress (*55*), which may be similar to the responses that we see here.

CONCLUSION

In summary, our results indicate that, normally, *flp-21*–dependent signaling of social cues (pheromones) increases maternal provisioning of translational components and reduces stress pathways such as RNAi and oxidative stress resistance. Our analyses indicate that *flp-21* is positioned upstream of the oxidative stress response and of maternal provisioning of translational components, which, in turn, is upstream of RNAi responsiveness. An intriguing possibility is that modulation of translation alone may be an efficient way to promote stress pathways, allowing these distinct responses to be coordinated.

MATERIALS AND METHODS
Worm maintenance
Worms were maintained according to Brenner (*56*) at 20°C unless otherwise indicated. Strains used are supplied in table S1.

RNAi
RNAi was conducted according to WormBook (*57*) by feeding L4 (fourth larval stage) larvae—young adult worm bacteria expressing dsRNA for 24 hours (unless otherwise stated). RNAi plates were generated according to Von Stetina *et al.* (*58*) as follows: EV (L4440 bacteria) and *pha-4* (PR244) were grown overnight at 37°C with antibiotic carbenicillin (50 μg/ml). OD_{600} (optical density at 600 nm) of 1:10 dilution of culture was checked, and then concentrated culture was diluted to OD_{600} 1.5 in LB. Cultures were centrifuged for 6 min at 4.4 rpm at room temperature, and the supernatant was removed. Bacteria were resuspended in 10% of original volume in LB. EV (L4440) and *pha-4* (PR244) cultures were mixed together to dilute the *pha-4* dsRNA, i.e., 1:4 or 1:5 of *pha-4* dsRNA bacteria to EV dsRNA bacteria. Bacteria (250 μl) were seeded onto nematode growth medium (NGM) plates and allowed to grow for 2 days at room temperature. Plates were placed at 4°C for 2 days before use. The dsRNA bacteria clones were from the Ahringer RNAi library (*59*). The identity of each clone was confirmed by sequencing before use. For other RNAi clones, bacteria were grown in 5 ml of LB with 5 μl of carbenicillin (100 mg/ml) for 6 to 8 hours at 37°C and pelleted at 2500*g* for 10 min. The bacterial pellet was resuspended in 400 μl of 0.5 M isopropyl-β-D-thiogalactopyranoside (IPTG), 30 μl of carbenicillin (100 mg/ml), and 70 μl of nuclease-free water. NGM plates (5 ml) were seeded with 200 μl of resuspended bacterial solution, kept at room temperature for 2 days, and then stored at 4°C overnight before use.

Survival assay
For each RNAi assay, wild-type control worms were evaluated in parallel to mutant test worms. L4 animals were placed on *pha-4* dsRNA plates at 25°C, unless otherwise indicated, for 24 hours (unless otherwise indicated). Embryos were removed from the RNAi plates and transferred to plates with OP50 and allowed to grow for 2 days at either 20° or 25°C, and the surviving adult animals were counted. For the statistics, the survival after test RNAi was normalized to the survival of EV counterparts (%EV survival). Statistics were performed according to the experimental design: Wilcoxon rank sum (one control to one mutant), analysis of variance (ANOVA)/Dunnett's (one control for two or more mutants), or ANOVA/Tukey's (epistasis experiments). For the graphing, wild type (normalized to %EV) for each experiment was set to 1 and mutant %EV survival was graphed as a ratio. Boxplots were graphed using ggplot2 geom_boxplot function.

Pheromone treatment
Generation of conditioned medium
Wild-type N2 worms were harvested by washing off 2 × 6 cm plates with S media and adding to 250 ml of cultures. These were grown in S media 250-ml cultures (following WormBook protocol: substituting sodium citrate for potassium citrate) (*60*) fed with a starting pellet of OP50 *E. coli* roughly equal to that from 500 ml of culture. Three cultures were started, kept at 25°C, and rotated at 180 rpm. One culture was harvested at 3 days, and the second culture at day 5. The remaining culture was fed again on day 5 and then on day 10, and subsequently harvested on day 12. Each feeding was roughly equal in size and done when the cultures began to become less hazy. To harvest each culture, the liquid from the culture was pelleted using a centrifuge at 6500 rpm for 20 min. The clarified medium was decanted and freeze-dried along with the pellet. The pellets were extracted with a 3:1 mixture of MeOH and $CHCl_3$, and the freeze-dried medium was extracted with MeOH and EtOH twice for ~100 ml in total. Because of the large amount of dissolved salts, the extracts were triturated with MeOH twice and filtered through a plug of celite. This procedure was only done with the medium extracts and not the extracts from the pellets. The ascaroside dauer pheromones, asc-C6-MK (C6; ascr#2), asc-ΔC9 (C9; ascr#3), and asc-ωC3 (C3; ascr#5), were synthesized according to previously published methods (*61*).

Pharyngeal pumping rate assays
Pumping assays were performed similarly as previously described (*62*). Briefly, young adults that were well fed were examined for their pumping rate per 20 s while on either *E. coli* OP50 lawns or *pha-4(RNAi)* bacterial lawns. Numbers of pumps per 20 s were counted. For each experiment, five young adult worms were analyzed. Two to 3 days of assays were performed per mutant genotype. Wild-type worms were tested in parallel on each experimental day. For *E. coli* OP50 food lawns, worms were placed on food and left for 1 hour before measuring pumping rates. For *pha-4(RNAi)* plates, adult worms were tested during their 24-hour exposure on 1:4 dilution *pha-4(RNAi)* bacteria. Mean ± SE, Student's *t* test. *$P < 0.05$, **$P < 0.01$, and ***$P < 0.001$.

Cloning of Minimal-Mos1-NeoR-Ptag-168::flp-21::unc-54 3′UTR
A ~2.5-kb promoter region of *tag-168* and a ~0.7-kb fragment of *unc-54* downstream region were amplified from genomic DNA and

cloned into the plasmid A2-pCFJ910-Minimal-Mos1-NeoR-MCS together with the 201–base pair (bp) complementary DNA (cDNA) fragment of *flp-21* to generate Minimal-Mos1-NeoR-Ptag-168::flp-21::unc-54 3′ untranslated region (3′UTR).

Generation of integrated line
Single-copy integration line of Minimal-Mos1-NeoR-Ptag-168::flp-21::unc-54 3′UTR was generated by following minimal Mos1 transposon (miniMos) insertion protocol in (*63*). Selection of F1 transgenic animals and F2 animals was aided by co-injection markers and G418 resistance. The insertion was confirmed by PCR and sequencing.

Time course for RNAi sensitivity
Forty L4 worms were placed on EV and *pha-4(RNAi)* plates at 25°C. After each indicated time point, 100 embryos were removed and placed on OP50 plates, and adult worms were moved to new RNAi plates. Survival was assayed as indicated above.

Antibody staining
Antibody staining was conducted essentially according to Von Stetina *et al.* (*58*). Rapidly growing worms and embryos were washed off plates with dH$_2$O at room temperature and then pelleted for 1 min at 4000 rpm. Worm pellets were washed twice with 500 μl of dH$_2$O at room temperature. Pellets were resuspended in 300 μl of dH$_2$O bleach solution (4.8 ml of bleach, 1 ml of 5 M NaOH, and 4.2 ml of dH$_2$O) and incubated for 3 min with constant vortexing at room temperature. The bleaching reaction was stopped by adding dH$_2$O up to 1.5 ml. Embryos were washed three times with 1 ml of 1× M9 buffer (*60*) at room temperature and spun down for 1 min at 4000 rpm. Embryos were pipetted onto slides and allowed to settle. Excess liquid was removed and replaced with 35 μl of fixation solution [2% paraformaldehyde in phosphate-buffered saline (PBS)]. Embryos were squished with a coverslip until ~10% burst and then placed into a hybridization chamber for 15 min at room temperature. Slides were placed on dry ice for at least 1 hour. A freeze/crack was performed by popping off the coverslip, and then the slides were plunged into ice-cold MeOH for 3 min. Samples were washed three times in tris-buffered saline (TBS) + Tween 20 [50 mM tris-HCl, 150 mM NaCl, and 0.05% Tween 20 (pH 7.6)] for 15 min. Blocking nonspecific binding was performed for 30 min at 15°C with 100 μl of TNB blocking solution [50 mM tris-Cl (pH 7.5) and 150 mM NaCl plus 1% normal goat serum]. Primary antibodies were diluted in TNB at indicated concentrations, and samples were incubated overnight at 15°C. Slides were washed three times in TBS for 5 min each. Secondary antibodies were diluted in TNB at 1:200 concentration, and 100 μl was added to slides. Slides were incubated at 15°C for 1 to 2 hours. Slides were washed three times in TBS for 5 min each. Eight microliters of 1:3 Vectashield (Thermo Fisher Scientific) 4′,6-diamidino-2-phenylindole (DAPI):PBS was added to samples and allowed to incubate for 5 min. A coverslip was placed on slides and sealed with nail polish. Antibodies against the following proteins were used: endogenous PHA-4 (1:1000) (*64*) and DLG-1 (1:500; Thermo Fisher Scientific, MA1-045).

Worm culture for embryo isolation
Early embryos were collected from adult worms by bleaching for 5 min in 5× bleach solution (see above). Isolated embryos were shaken at 170 rpm at 20°C in Complete S Medium [100 mM NaCl, 5.6 mM K$_2$HPO$_4$, 4.4 mM KH$_2$PO$_4$, cholesterol (10 μg/ml), 10 mM potassium citrate, 2 mM CaCl$_2$, 2 mM MgSO$_4$, and 1× trace metals] without food overnight. Once the embryos hatched and became L1 larvae, concentrated NA22 bacteria were added to the culture. Synchronized embryos were harvested by bleaching after ~64 hours of growth when most worms carried one to two embryos, frozen in liquid nitrogen, and stored at −80°C (*65, 66*).

Total RNA isolation
Embryo pellets were resuspended in 100 μl of minimal salts solution (M9) (*65*) and 1 ml of TRIzol Reagent (Thermo Fisher Scientific, 15596026), then snap-frozen in liquid N$_2$, and stored at −80°C until all samples were collected. Tubes were placed in a 37°C heat block to warm just until thawed, with intermittent vortexing. Once samples were barely thawed, they were snap-frozen in liquid N$_2$, creating one freeze-thaw cycle. This was repeated four times. Debris was cleared by centrifuging samples at 12,000*g* for 10 min at 4°C. The supernatant was transferred to a new tube and incubated for 5 min at room temperature. BCP (1-bromo-3-chloropropane) (100 μl) was added, and samples were vortexed for 15 s. Samples were incubated for 2 to 3 min at room temperature and spun for 30 min at 12,000*g* at 4°C. The aqueous layer was transferred to a new tube, and 500 μl of 4°C isopropanol with 1 μl GlycoBlue (Thermo Fisher Scientific) was added to precipitate the RNA. Samples were placed at −20°C overnight. The next day, samples were spun for 25 min at 12,000*g* at 4°C. The RNA pellet was washed with 500 μl of cold 75% ethanol and then spun at 5 min at 12,000*g* at 4°C. The RNA pellet was air-dried in a fume hood and resuspended in 20 μl of nuclease-free water. Concentration and quality were measured on Bioanalyzer.

Sequencing analysis
Libraries were subjected to single-end sequencing with 50-bp read length on an Illumina HiSeq 2000 platform. Data processing and analyses were performed using the statistical programming environment R. Illumina TruSeq universal primer sequence (AGATC-GGAAGAGCACACGTCTGAACTCCAGTCAC) was trimmed using Cutadapt. mRNA libraries were mapped to the *C. elegans* genome (WBcel235) using Burrows-Wheeler Alignment Tool (BWA) and processed with SAMtools (*67, 68*). featureCounts (*69*) was used to count all alignments. Multiread correction was used on all mRNA read counts. mRNA read counts from each library were normalized to the total number of mapped reads. A variance stabilizing transformation was used before proceeding with downstream analysis. Each library was analyzed for differential expression using Deseq2 (*70*). $P < 0.05$ and log$_2$ fold change of 0.67 were used as cutoffs for differential expression. PCA loadings were calculated using rpm values. The variance captured in each principal component was extracted, and the correlation between each gene and each principal component was determined. The gene contribution projections of the top six genes were determined and graphed in Fig. 3. GO term enrichment was analyzed using DAVID (Database for Annotation, Visualization, and Integrated Discovery) and plotted using GOplot (*71*).

Quantitative PCR
cDNA was generated from total RNA using Maxima H Minus first-strand cDNA synthesis with dsDNase Kit (Thermo Fisher Scientific, K1681) with 1 μg of RNA from each sample. RNA was DNase-treated for 2 min at 37°C in a preheated thermomixer and then chilled on

ice after brief centrifugation. The first-strand cDNA synthesis reaction was performed in the same tube according to company recommendations, following reverse transcription PCR (RT-PCR) or RT-qPCR protocols. For qPCR, 1 µl of a 1:2 dilution of cDNA reaction was added to qRT reaction. qRT-PCR was carried out with an Eppendorf Mastercycler ep realplex using PowerUp SYBR Green Master Mix (Thermo Fisher Scientific, A25780). The following program was used for qPCR: 3 min at 95°C (3 s at 95°C, 15 s at 55°C, and 30 s at 72°C) for 40 cycles, followed by a melting curve. RT reactions without the enzyme and water served as negative controls. All reactions were done in triplicate and on two biological replicates. All the values were normalized to *act-1* as an internal control and to the transcript levels in untreated wild type via the $\Delta\Delta C_t$ method (*72*). Primer sequences used are in table S2.

^{35}S metabolic labeling

^{35}S metabolic labeling was conducted according to Hansen *et al.* (*40*). Worms were synchronized in M9 buffer, and 1000 L1 larvae were plated on fresh OP50 plates and allowed to grow to young adulthood before they produced embryos (~2 days). Ten plates per genotype were grown for each assay plus an additional 10 plates for negative controls. OP50 cultures were grown overnight for a maximum of 12 hours at 37°C: One culture was grown in LB, and one culture with ^{35}S methionine at 10 µCi/ml (PerkinElmer). The next day, OP50 cultures were spun down and concentrated 10×. Worms were harvested by washing with S basal (*60*) and settling on ice. Worms were washed with 1× S basal and then with 1× S media (*60*). Total volume was brought down to 2 ml with 200 µM 5-fluoro-2′-deoxyuridine (to prevent embryo production; Sigma-Aldrich, F0503). Radioactive OP50 (100 µl) was added to test samples, and 100 µl of nonradioactive OP50 was added to control samples and then shaken at room temperature for 5 hours. Samples were then washed with 1× S basal and 1× S media, and volume was brought down to 2 ml. For negative control samples, 100 µl of radioactive bacteria was added for less than 1 min with shaking and then washed as previously described. Unlabeled OP50 (100 µl) was added to samples and then shaken at room temperature for 30 min to purge radioactive bacteria out of the intestine. Two hundred microliters of 1% SDS was added, and samples were boiled for 15 min using a heat block set at 100°C and mixed every 5 min for 15 min. Samples were spun at 14,000 rpm for 15 min, and the supernatant was removed and placed in new tube. The supernatant was precipitated with 10% trichloroacetic acid (Sigma-Aldrich, T0699) on ice for 1 hour. Protein was collected by centrifugation at 14,000 rpm and washed with ice-cold ethanol. After air drying, protein pellets were resuspended in 1% SDS. Protein concentration was measured using a spectrophotometer (NanoDrop) and bicinchoninic acid protein assay kit. Sample (20 µl) was taken in duplicate for ^{35}S count taken by Beckman scintillation counter. ^{35}S incorporation levels were calculated by normalizing ^{35}S counts per minute, corrected for unspecific background ($t = 0$), to total protein levels. Statistical analysis was done as one-sided, paired Student's t test on the ^{35}S incorporation levels. The relative ^{35}S incorporation (used for plotting) was calculated by normalizing the ^{35}S incorporation levels of a given mutant to the ^{35}S incorporation levels of the control/wild type, which was set to 100.

Single-molecule FISH

smFISH was conducted as described in previous studies (*73*). Worms and embryos were washed off rapidly growing plates with

dH_2O at room temperature and then pelleted for 1 min at 4000 rpm. Worm pellets were washed three times with 150 µl of dH_2O at room temperature. Pellets were resuspended in 150 µl of dH_2O bleach solution (4.8 ml of bleach, 1 ml of 5 M NaOH, and 4.2 ml of dH_2O) and incubated for 4.5 min at 25°C in a thermomixer. The bleaching reaction was stopped by adding dH_2O up to 1.5 ml. Embryos were washed three times with 150 µl of 1× M9 at room temperature and spun down for 1 min at 4000 rpm. Embryos were pipetted onto slides and allowed to settle. Excess liquid was removed and replaced with 35 µl of fixation solution (3.7% formaldehyde in 1× PBS/0.05% Triton X-100). Embryos were squished with a coverslip until ~10% burst and then placed into a hybridization chamber for 5 min at room temperature. Slides were placed on dry ice for at least 1 hour. A freeze/crack was performed by popping off the coverslip, and then the slides were plunged into ice-cold MeOH for 5 min. Samples were washed twice in PBS for 5 min and three times in PBS-0.5% Triton X-100 for 15 min. Blocking was performed for 1 hour at 37°C with 100 µl of smFISH hybridization buffer probes (3.7% formaldehyde in 1× PBS/0.05% Triton X-100).

RNA FISH probes

RNA probes were made by Integrated DNA Technologies. Primary probe solution (2 µl of FLAPY probe + 98 µl of hybridization buffer) was added to samples and incubated in a humidity chamber at 37°C for 5 hours. Embryos were washed three times in smFISH wash buffer (10% formamide in 2× SSC/0.5% Triton X-100) for 5 min each. Embryos were washed for 1 hour at 37°C. Samples were washed twice more in smFISH wash buffer for 5 min each. Eight microliters of 1:3 Vectashield (Thermo Fisher Scientific) DAPI:PBS was added to samples and allowed to incubate for 5 min. A coverslip was placed on slides and sealed with nail polish. smFISH analysis was performed using the FISH-quant program (*74*). smFISH foci were localized in 3D space using Gaussian fitting. Quality control for localized spot is determined by its point spread function. Embryos were staged by counting the number of DAPI nuclei.

Oxidative stress assay

Thirty L4 stage worms were placed in 100 µl of either 1.7 or 2.3 mM H_2O_2 solution in cell culture plates according to Chávez *et al.* (*52*). Worms were assayed every 1.5 hours for survival by prodding and assessing movement of either worm body or pharyngeal pumping.

Note added in proof: M. Francisco Perez, M. Shamalnasab, A. Mata-Cabana, S. Della Valle, M. Olmedo, M. Francesconi, B. Lehner. Neuronal perception of the social environment generates an inherited memory that controls the development and generation time of *C. elegans*. *Current Biology* **31**, 1–13, August 5, 2021.

REFERENCES AND NOTES

1. M. F. Perez, B. Lehner, Vitellogenins—Yolk gene function and regulation in *Caenorhabditis elegans*. *Front. Physiol.* **10**, 1067 (2019).
2. R. Posner, I. A. Toker, O. Antonova, E. Star, S. Anava, E. Azmon, M. Hendricks, S. Bracha, H. Gingold, O. Rechavi, Neuronal small RNAs control behavior transgenerationally. *Cell* **177**, 1814–1826.e15 (2019).

3. S. Devanapally, S. Ravikumar, A. M. Jose, Double-stranded RNA made in *C. elegans* neurons can enter the germline and cause transgenerational gene silencing. *Proc. Natl. Acad. Sci. U.S.A.* **112**, 2133–2138 (2015).

4. A. C. Billi, S. E. J. Fischer, J. K. Kim, Endogenous RNAi pathways in *C. elegans*. *WormBook*, 1–49 (2014).

5. J. W. Golden, D. L. Riddle, A gene affecting production of the *Caenorhabditis elegans* dauer-inducing pheromone. *Mol. Gen. Genet.* **198**, 534–536 (1985).

6. R. A. Butcher, J. R. Ragains, W. Li, G. Ruvkun, J. Clardy, H. Y. Mak, Biosynthesis of the *Caenorhabditis elegans* dauer pheromone. *Proc. Natl. Acad. Sci. U.S.A.* **106**, 1875–1879 (2009).

7. R. A. Butcher, M. Fujita, F. C. Schroeder, J. Clardy, Small-molecule pheromones that control dauer development in *Caenorhabditis elegans*. *Nat. Chem. Biol.* **3**, 420–422 (2007).

8. X. Zhang, L. Feng, S. Chinta, P. Singh, Y. Wang, J. K. Nunnery, R. A. Butcher, Acyl-CoA oxidase complexes control the chemical message produced by *Caenorhabditis elegans*. *Proc. Natl. Acad. Sci. U.S.A.* **112**, 3955–3960 (2015).

9. P.-Y. Jeong, M. Jung, Y.-H. Yim, H. Kim, M. Park, E. Hong, W. Lee, Y. H. Kim, K. Kim, Y.-K. Paik, Chemical structure and biological activity of the *Caenorhabditis elegans* dauer-inducing pheromone. *Nature* **433**, 541–545 (2005).

10. R. A. Butcher, J. R. Ragains, E. Kim, J. Clardy, A potent dauer pheromone component in *Caenorhabditis elegans* that acts synergistically with other components. *Proc. Natl. Acad. Sci. U.S.A.* **105**, 14288–14292 (2008).

11. J. Q. White, E. M. Jorgensen, Sensation in a single neuron pair represses male behavior in hermaphrodites. *Neuron* **75**, 593–600 (2012).

12. J. S. Greene, M. Brown, M. Dobosiewicz, I. G. Ishida, E. Z. Macosko, X. Zhang, R. A. Butcher, D. J. Cline, P. T. McGrath, C. I. Bargmann, Balancing selection shapes density-dependent foraging behaviour. *Nature* **539**, 254–258 (2016).

13. K. Kim, K. Sato, M. Shibuya, D. M. Zeiger, R. A. Butcher, J. R. Ragains, J. Clardy, K. Touhara, P. Sengupta, Two chemoreceptors mediate developmental effects of dauer pheromone in *C. elegans*. *Science* **326**, 994–998 (2009).

14. J. Srinivasan, F. Kaplan, R. Ajredini, C. Zachariah, H. T. Alborn, P. E. A. Teal, R. U. Malik, A. S. Edison, P. W. Sternberg, F. C. Schroeder, A blend of small molecules regulates both mating and development in *Caenorhabditis elegans*. *Nature* **454**, 1115–1118 (2008).

15. E. Z. MacOsko, N. Pokala, E. H. Feinberg, S. H. Chalasani, R. A. Butcher, J. Clardy, C. I. Bargmann, A hub-and-spoke circuit drives pheromone attraction and social behaviour in *C. elegans*. *Nature* **458**, 1171–1175 (2009).

16. L. Ryu, Y. Cheon, Y. H. Huh, S. Pyo, S. Chinta, H. Choi, R. A. Butcher, K. Kim, Feeding state regulates pheromone-mediated avoidance behavior via the insulin signaling pathway in *Caenorhabditis elegans*. *EMBO J.* **37**, e98402 (2018).

17. B. C. Prasad, B. Ye, R. Zackhary, K. Schrader, G. Seydoux, R. R. Reed, unc-3, a gene required for axonal guidance in *Caenorhabditis elegans*, encodes a member of the O/E family of transcription factors. *Development* **125**, 1561–1568 (1998).

18. K. Kim, M. E. Colosimo, H. Yeung, P. Sengupta, The UNC-3 Olf/EBF protein represses alternate neuronal programs to specify chemosensory neuron identity. *Dev. Biol.* **286**, 136–148 (2005).

19. S. J. Husson, E. Clynen, G. Baggerman, T. Janssen, L. Schoofs, Defective processing of neuropeptide precursors in *Caenorhabditis elegans* lacking proprotein convertase 2 (KPC-2/EGL-3): Mutant analysis by mass spectrometry. *J. Neurochem.* **98**, 1999–2012 (2006).

20. W. L. Hung, Y. Wang, J. Chitturi, M. Zhen, A *Caenorhabditis elegans* developmental decision requires insulin signaling-mediated neuron-intestine communication. *Development* **141**, 1767–1779 (2014).

21. C. Li, K. Kim, Neuropeptides. *WormBook*, 1–36 (2008).

22. C. Thacker, K. Peters, M. Srayko, A. M. Rose, The bli-4 locus of *Caenorhabditis elegans* encodes structurally distinct kex2/subtilisin-like endoproteases essential for early development and adult morphology. *Genes Dev.* **9**, 956–971 (1995).

23. D. Sieburth, J. M. Madison, J. M. Kaplan, PKC-1 regulates secretion of neuropeptides. *Nat. Neurosci.* **10**, 49–57 (2007).

24. S. Speese, M. Petrie, K. Schuske, M. Ailion, K. Ann, K. Iwasaki, E. M. Jorgensen, T. F. J. Martin, UNC-31 (CAPS) is required for dense-core vesicle but not synaptic vesicle exocytosis in *Caenorhabditis elegans*. *J. Neurosci.* **27**, 6150–6162 (2007).

25. G. A. Lemieux, K. A. Cunningham, L. Lin, F. Mayer, Z. Werb, K. Ashrafi, Kynurenic acid is a nutritional cue that enables behavioral plasticity. *Cell* **160**, 119–131 (2015).

26. C. Rogers, V. Reale, K. Kim, H. Chatwin, C. Li, P. Evans, M. De Bono, Inhibition of *Caenorhabditis elegans* social feeding by FMRFamide-related peptide activation of NPR-1. *Nat. Neurosci.* **6**, 1178–1185 (2003).

27. J. D. Hibshman, A. Hung, L. R. Baugh, Maternal diet and insulin-like signaling control intergenerational plasticity of progeny size and starvation resistance. *PLOS Genet.* **12**, e1006396 (2016).

28. J. M. Jordan, J. D. Hibshman, A. K. Webster, R. E. W. Kaplan, A. Leinroth, R. Guzman, C. S. Maxwell, R. Chitrakar, E. A. Bowman, A. L. Fry, E. J. A. Hubbard, L. R. Baugh, Insulin/ IGF signaling and vitellogenin provisioning mediate intergenerational adaptation to nutrient stress. *Curr. Biol.* **29**, 2380–2388.e5 (2019).

29. N. O. Burton, T. Furuta, A. K. Webster, R. E. W. Kaplan, L. R. Baugh, S. Arur, H. R. Horvitz, Insulin-like signalling to the maternal germline controls progeny response to osmotic stress. *Nat. Cell Biol.* **19**, 252–257 (2017).

30. Y. Kushibiki, T. Suzuki, Y. Jin, H. Taru, RIMB-1/RIM-binding protein and UNC-10/RIM redundantly regulate presynaptic localization of the voltage-gated calcium channel in *Caenorhabditis elegans*. *J. Neurosci.* **39**, 8617–8631 (2019).

31. K. Peymen, J. Watteyne, L. Frooninckx, L. Schoofs, I. Beets, The FMRFamide-like peptide family in nematodes. *Front. Endocrinol.* **5**, 90 (2014).

32. M. R. Lackner, S. J. Nurrish, J. M. Kaplan, Facilitation of synaptic transmission by EGL-30 $G_q\alpha$ and EGL-8 PLCβ: DAG binding to UNC-13 is required to stimulate acetylcholine release. *Neuron* **24**, 335–346 (1999).

33. Y. M. Hajdu-Cronin, W. J. Chen, G. Patikoglou, M. R. Koelle, P. W. Sternberg, Antagonism between $G_o\alpha$ and $G_q\alpha$ in *Caenorhabditis elegans*: The RGS protein EAT-16 is necessary for $G_o\alpha$ signaling and regulates $G_q\alpha$ activity. *Genes Dev.* **13**, 1780–1793 (1999).

34. S. C. Tintori, E. O. Nishimura, P. Golden, J. D. Lieb, B. Goldstein, A transcriptional lineage of the early *C. elegans* embryo. *Dev. Cell* **38**, 430–444 (2016).

35. J. P. Lim, A. Brunet, Bridging the transgenerational gap with epigenetic memory. *Trends Genet.* **29**, 176–186 (2013).

36. P. Svoboda, V. Franke, R. M. Schultz, Sculpting the transcriptome during the oocyte-to-embryo transition in mouse. *Curr. Top. Dev. Biol.* **113**, 305–349 (2015).

37. N. L. Vastenhouw, W. X. Cao, H. D. Lipshitz, The maternal-to-zygotic transition revisited. *Development* **146**, dev161415 (2019).

38. M. Levin, T. Hashimshony, F. Wagner, I. Yanai, Developmental milestones punctuate gene expression in the *Caenorhabditis* embryo. *Dev. Cell* **22**, 1101–1108 (2012).

39. M. S. Sengupta, W. Y. Low, J. R. Patterson, H.-M. Kim, A. Traven, T. H. Beilharz, M. P. Colaiacovo, J. A. Schisa, P. R. Boag, ifet-1 is a broad-scale translational repressor required for normal P granule formation in *C. elegans*. *J. Cell Sci.* **126**, 850–859 (2013).

40. M. Hansen, S. Taubert, D. Crawford, N. Libina, S.-J. Lee, C. Kenyon, Lifespan extension by conditions that inhibit translation in *Caenorhabditis elegans*. *Aging Cell* **6**, 95–110 (2007).

41. H. Li, C. Ren, J. Shi, X. Hang, F. Zhang, Y. Gao, Y. Wu, L. Xu, C. Chen, C. Zhang, A proteomic view of *Caenorhabditis elegans* caused by short-term hypoxic stress. *Proteome Sci.* **8**, 49 (2010).

42. M. Hanazawa, I. Kawasaki, H. Kunitomo, K. Gengyo-ando, The *Caenorhabditis elegans* eukaryotic initiation factor 5A homologue, IFF-1, is required for germ cell proliferation, gametogenesis and localization of the P-granule component PGL-1. *Mech. Dev.* **121**, 213–224 (2004).

43. A. P. Schuller, C. C.-C. Wu, T. E. Dever, A. R. Buskirk, R. Green, eIF5A functions globally in translation elongation and termination. *Mol. Cell* **66**, 194–205.e5 (2017).

44. N. Kedersha, G. Stoecklin, M. Ayodele, P. Yacono, J. Lykke-andersen, J. F. Marvin, D. Scheuner, R. J. Kaufman, D. E. Golan, P. Anderson, Stress granules and processing bodies are dynamically linked sites of mRNP remodeling. *J. Cell Biol.* **169**, 871–884 (2005).

45. G.-Q. Wu, Y.-M. Xu, A. T. Y. Lau, Recent insights into eukaryotic translation initiation factors 5A1 and 5A2 and their roles in human health and disease. *Cancer Cell Int.* **20**, 142 (2020).

46. T. K. Blackwell, A. K. Sewell, Z. Wu, M. Han, TOR signaling in *Caenorhabditis elegans* development, metabolism, and aging. *Genetics* **213**, 329–360 (2019).

47. T. R. Fenton, I. T. Gout, Functions and regulation of the 70kDa ribosomal S6 kinases. *Int. J. Biochem. Cell Biol.* **43**, 47–59 (2011).

48. K. Z. Pan, J. E. Palter, A. N. Rogers, A. Olsen, D. Chen, G. J. Lithgow, P. Kapahi, Inhibition of mRNA translation extends lifespan in *Caenorhabditis elegans*. *Aging Cell* **6**, 111–119 (2007).

49. P. Syntichaki, K. Troulinaki, N. Tavernarakis, eIF4E function in somatic cells modulates ageing in *Caenorhabditis elegans*. *Nature* **445**, 922–926 (2007).

50. A. R. Mansisidor, G. Cecere, S. Hoersch, M. B. Jensen, T. Kawli, L. M. Kennedy, V. Chavez, M.-W. Tan, J. D. Lieb, A. Grishok, A conserved PHD finger protein and endogenous RNAi modulate insulin signaling in *Caenorhabditis elegans*. *PLOS Genet.* **7**, e1002299 (2011).

51. V. Singh, A. Aballay, Heat shock and genetic activation of HSF-1 enhance immunity to bacteria. *Cell Cycle* **5**, 2443–2446 (2006).

52. V. Chávez, A. Mohri-Shiomi, A. Maadani, L. A. Vega, D. A. Garsin, Oxidative stress enzymes are required for daf-16-mediated immunity due to generation of reactive oxygen species by *Caenorhabditis elegans*. *Genetics* **176**, 1567–1577 (2007).

53. C. D. Chute, E. M. DiLoreto, Y. K. Zhang, D. K. Reilly, D. Rayes, V. L. Coyle, H. J. Choi, M. J. Alkema, F. C. Schroeder, J. Srinivasan, Co-option of neurotransmitter signaling for inter-organismal communication in *C. elegans*. *Nat. Commun.* **10**, 3186 (2019).

54. R. Pocock, O. Hobert, Hypoxia activates a latent circuit for processing gustatory information in *C. elegans*. *Nat. Neurosci.* **13**, 610–614 (2010).

55. G. A. Carrasco, L. D. Van de Kar, Neuroendocrine pharmacology of stress. *Eur. J. Pharmacol.* **463**, 235–272 (2003).

56. S. Brenner, The genetics of *Caenorhabditis elegans*. *Genetics* **77**, 71–94 (1974).

57. J. Ahringer, Reverse genetics. *WormBook*, 1–43 (2006).

58. S. E. Von Stetina, J. Liang, G. Marnellos, S. E. Mango, Temporal regulation of epithelium formation mediated by FoxA, MKLP1, MgcRacGAP, and PAR-6. *Mol. Biol. Cell* **28**, 2042–2065 (2017).

59. R. S. Kamath, J. Ahringer, Genome-wide RNAi screening in *Caenorhabditis elegans*. *Methods* **30**, 313–321 (2003).

60. T. Stiernagle, Maintenance of *C. elegans*. *WormBook*, 1–11 (2006).

61. K. A. Hollister, E. S. Conner, X. Zhang, M. Spell, G. M. Bernard, P. Patel, A. C. G. V. de Carvalho, R. A. Butcher, J. R. Ragains, Ascaroside activity in *Caenorhabditis elegans* is highly dependent on chemical structure. *Bioorg. Med. Chem* **21**, 5754–5769 (2013).

62. D. Raizen, B.-M. Song, N. Trojanowski, Y.-J. You, Methods for measuring pharyngeal behaviors. *WormBook*, 1–13 (2012).

63. C. Frøkjær-Jensen, M. W. Davis, M. Sarov, J. Taylor, S. Flibotte, M. LaBella, A. Pozniakovsky, D. G. Moerman, E. M. Jorgensen, Random and targeted transgene insertion in *Caenorhabditis elegans* using a modified Mos1 transposon. *Nat. Methods* **11**, 529–534 (2014).

64. J. Gaudet, S. E. Mango, Regulation of organogenesis by the *Caenorhabditis elegans* FoxA protein PHA-4. *Science* **295**, 821–825 (2002).

65. B. Mutlu, H.-M. Chen, S. Gutnik, D. H. Hall, S. Keppler-Ross, S. E. Mango, Distinct functions and temporal regulation of methylated histone H3 during early embryogenesis. *Development* **146**, dev174516 (2019).

66. B. Mutlu, H.-M. Chen, J. J. Moresco, B. D. Orelo, B. Yang, J. M. Gaspar, S. Keppler-Ross, J. R. Yates III, D. H. Hall, E. M. Maine, S. E. Mango, Regulated nuclear accumulation of a histone methyltransferase times the onset of heterochromatin formation in *C. elegans* embryos. *Sci. Adv.* **4**, eaat6224 (2018).

67. H. Li, R. Durbin, Fast and accurate short read alignment with Burrows-Wheeler transform. *Bioinformatics* **25**, 1754–1760 (2009).

68. H. Li, B. Handsaker, A. Wysoker, T. Fennell, J. Ruan, N. Homer, G. Marth, G. Abecasis, R. Durbin; 1000 Genome Project Data Processing Subgroup, The Sequence Alignment/ Map format and SAMtools. *Bioinformatics* **25**, 2078–2079 (2009).

69. Y. Liao, G. K. Smyth, W. Shi, The Subread aligner: Fast, accurate and scalable read mapping by seed-and-vote. *Nucleic Acids Res.* **41**, e108 (2013).

70. M. I. Love, W. Huber, S. Anders, Moderated estimation of fold change and dispersion for RNA-seq data with DESeq2. *Genome Biol.* **15**, 550 (2014).

71. W. Walter, F. Sánchez-Cabo, M. Ricote, GOplot: An R package for visually combining expression data with functional analysis. *Bioinformatics* **31**, 2912–2914 (2015).

72. T. D. Schmittgen, K. J. Livak, Analyzing real-time PCR data by the comparative CT method. *Nat. Protoc.* **3**, 1101–1108 (2008).

73. N. Ji, A. Van Oudenaarden, Single molecule fluorescent in situ hybridization (smFISH) of *C. elegans* worms and embryos. *WormBook*, 1–16 (2012).

74. N. Tsanov, A. Samacoits, R. Chouaib, A.-M. Traboulsi, T. Gostan, C. Weber, C. Zimmer, K. Zibara, T. Walter, M. Peter, E. Bertrand, F. Mueller, smiFISH and FISH-quant - A flexible single RNA detection approach with super-resolution capability. *Nucleic Acids Res.* **44**, e165 (2016).

Citation: J. A. Wasson, G. Harris, S. Keppler-Ross, T. J. Brock, A. R. Dar, R. A. Butcher, S. E. J. Fischer, K. Kagias, J. Clardy, Y. Zhang, S. E. Mango, Neuronal control of maternal provisioning in response to social cues. *Sci. Adv.* **7**, eabf8782 (2021).

Science Advances

Neuronal control of maternal provisioning in response to social cues

Jadiel A. Wasson, Gareth Harris, Sabine Keppler-Ross, Trisha J. Brock, Abdul R. Dar, Rebecca A. Butcher, Sylvia E. J. Fischer, Konstantinos Kagias, Jon Clardy, Yun Zhang and Susan E. Mango

ARTICLE TOOLS	http://advances.sciencemag.org/content/7/34/eabf8782
SUPPLEMENTARY MATERIALS	http://advances.sciencemag.org/content/suppl/2021/08/16/7.34.eabf8782.DC1
REFERENCES	This article cites 68 articles, 22 of which you can access for free http://advances.sciencemag.org/content/7/34/eabf8782#BIBL
PERMISSIONS	http://www.sciencemag.org/help/reprints-and-permissions

Use of this article is subject to the Terms of Service